# Ferroelectric nanodomains in epitaxial GeTe thin films

Boris Croes, Fabien Cheynis, Yide Zhang, Cédric Voulot, Kokou Dodzi Dorkenoo, Salia Cherifi-Hertel, Cristian Mocuta, Michaël Texier, Thomas W. Cornelius, Olivier Thomas, et al.

# Ferroelectric nanodomains in epitaxial GeTe thin films

Boris Croes,[1] Fabien Cheynis,[1] Yide Zhang,[2] Cédric Voulot,[2] Kokou Dodzi Dorkenoo,[2] Salia Cherifi-Hertel,[2] Cristian Mocuta,[3] Michaël Texier,[4] Thomas Cornelius,[4] Olivier Thomas,[4] Marie-Ingrid Richard,[5] Pierre Müller,[1] Stefano Curiotto,[1] and Frédéric Leroy[1]

[1] *Aix Marseille Univ, CNRS, CINAM, AMUTECH, Marseille, France*
[2] *Université de Strasbourg, CNRS, Institut de Physique et Chimie des Matériaux de Strasbourg, Strasbourg, 67000, France*
[3] *Synchrotron SOLEIL, L'Orme des Merisiers, St Aubin BP 48, F-91192 Gif Sur Yvette, France*
[4] *Aix Marseille Univ, Univ Toulon, IM2NP, AMUTECH, CNRS, F-13397 Marseille 20, France*
[5] *Univ Grenoble Alpes, CEA Grenoble, IRIG, MEM, NRS, 17 Rue Martyrs, F-38000 Grenoble, France*

(Dated: July 29, 2021)

In the quest for materials for ferroelectrics-based spintronics with a large spin-orbit coupling, it is essential to carefully control the ferroelectric domains structure, their spatial organization and the domain wall type. Here, we perform the growth of GeTe thin films on Si by molecular beam epitaxy in a large thickness range. We show that the volume fraction along with the size of the ferroelectric nanodomains can be controlled by finely adjusting the deposition thickness and temperature. We evidence the formation of 71°-type domain walls and *in situ* measurements during thermal cycling show the hysteretic appearance and decay of ferroelectric domains. In combination with a detailed analysis of the GeTe/Si interface, we demonstrate that the interfacial misfit dislocations formed during the growth plays a key role in the stability of the ferroelectric nanodomains.

PACS numbers: GeTe, ferroelectrics, domain wall

## I. INTRODUCTION

The epitaxial growth of thin films on single crystal substrates often leads to the development of strain fields. In ferroelectrics, this provides an extra degree of freedom to control their structure, ferroelectric transition temperature, and related functionalities such as optical, dielectric and piezoelectric responses [1–3]. The domain structure plays a central role in the relaxation mechanisms, owing to its strong dependence on tensile or compressive strain that is imposed by the substrate. Recently, strain engineering, by the selection of appropriate substrates, and the control of charge screening in thin films and superlattices has led to the discovery of new ferroelectric phases showing exotic domain patterns and polarization textures.[4–8] Furthermore, strain relaxation in thick films is often accompanied by the formation of ferroelastic domains and twin boundaries which can add further functionalization [9] *via* self-organized domain patterns [10–12].

Among ferroelectrics a new class of materials with high potentialities for spintronic applications has recently been introduced as ferroelectric Rashba semiconductors (FERSCs) [13 and 14]. Main results, obtained on $\alpha$-GeTe thin films, have demonstrated that the reversal of the ferroelectric polarization under an electric field leads to a consistent change in the spin chirality of the band structure [15 and 16]. An effective spin-to-charge conversion has also been demonstrated in a ferromagnetic-GeTe heterostructure [17 and 18] and a nonreciprocal charge transport up to room temperature has been detected [19]. All these advances pave the way for an all-electric spintronics based on semiconducting materials. However the influence of the domain structure on these phenomena still remains unclear. Given the rhombohedral structure of GeTe (R3m space group) and the existence of an electric dipole in the $\langle 111 \rangle$ direction, eight possible polar domain orientations are anticipated in this system. This was unambiguously confirmed by the observation of herringbone domain configurations in low-temperature $\alpha$-phase GeTe crystals[20 and 21]. In the context of epitaxial (111)-oriented thin films a dominant self-poled state with a polarization perpendicular to the surface has been evidenced [15, 16, and 22]. However a few results [23 and 24] indicate that this is a simplified view and minority incursions occur in thin films. In spite of the growing interest in such ferroelectric Rashba semiconductors [25 and 26], the detailed polar domain structure and spatial organization has not been studied so far. These studies are a prerequisite for the controlled switching of ferroelectric domains and the understanding of aging properties.

In this article we address the ferroelectric nanodomains organization of $\alpha$-GeTe thin films grown on Si(111), the domain wall type, and the structure of the interface with the substrate. As reported by Wang et al. [23], quasi-single crystalline $\alpha$-GeTe thin films can be grown on Si(111) by molecular beam epitaxy using a pre-deposition of 1 monolayer (ML) of Sb onto the substrate. It is an ideal platform to study and control ferroelectric domains as they are no more limited by grain boundaries. We have determined by X-ray diffraction (three-dimensional reciprocal space maps) in combination with low energy electron microscopy (LEEM) the volume fraction of the ferroelectric domains and the domains size in a large range of film thickness (10-1800 nm). Second harmonic generation (SHG) microscopy combined to polarimetry analysis reveal the local symmetry of these domains. Using high resolution transmission electron microscopy (HR-

TEM) we show that domain walls are only of 71°-type and that the GeTe/Si interface is stabilized by misfit dislocations that relax the large lattice parameter mismatch between both lattices. The reversible decay/growth of the ferroelectric nanodomains under annealing/cooling, as demonstrated by *in situ* LEEM, is attributed to the thermal stress induced by the large difference of linear thermal expansion coefficients of both materials.

## II. METHODS

### Sample preparation and GeTe thin film growth by molecular beam epitaxy

Si(111) wafers (Siltronix; 550 $\mu$m -thick; $\rho$=1-10 $\Omega$cm) are first cleaned by acetone and ethanol rising before introduction in ultra high vacuum (UHV, P<$10^{-7}$ Pa). Then the substrates are degased at 1000 K during 12 h followed by repeated high temperature annealing (1500 K) during a few minutes in order to achieve a clean 7×7 surface reconstruction. Finally a deposition of 1 ML of Sb is performed on the Si(111) surface, forming the so-called Si(111)-$\sqrt{3}\times\sqrt{3}$-Sb reconstruction [27] that greatly improves the crystalline quality of the GeTe layer [23]. The GeTe thin films are grown by co-deposition of Ge (1100 °C) and Te (310 °C) in UHV at 275°C and characterized by *in situ* reflection high energy electron diffraction (RHEED). All the deposition sources are effusion cells from MBE-Komponenten.

### LEEM and LEED surface characterization of nanodomains

After growth the GeTe layers are transferred under UHV conditions and characterized by low energy electron microscopy and low energy electron diffraction (LEEM III, Elmitec GmbH). LEEM images were obtained in bright field mode at an incident energy of 26 eV where a local maximum of reflectivity occurs. At this energy the reflected beams by the GeTe main domain and by the tilted ferroelectric nanodomains are clearly separated in the focal plane. This allows to use either the medium contrast aperture (Ø=30 $\mu$m) to select all reflected beams or the smallest contrast aperture (Ø=10 $\mu$m) to select only the reflected beam from the main domain. In situ LEEM characterization of the domains evolution under thermal treatments were performed with temperature steps of 10° C and waiting time of 30 min for stabilization.

### X-ray diffraction and 3D reciprocal space maps

The internal structure of GeTe thin films has been studied by X-ray diffraction at DiffAbs beamline (Synchrotron SOLEIL). X-ray diffraction data have been measured at 9.5 keV [0.13051 nm] and 16.9 keV [0.07336 nm]. The incident beam was focused on the sample surface to a size of 250 × 300 $\mu m^2$. The diffracted intensity was collected onto a 2D XPAD hybrid pixel detector. Three-dimensional reciprocal space maps of the GeTe $222_c$ Bragg reflection were recorded by rocking the sample by ±3°. The typical step was about 0.01°. The data analysis consists of a flat field correction (of the possible non-uniform response of the various pixels of the detector) and then a conversion of the measured data from the detector coordinates (pixel index) to diffraction angles and thus to reciprocal space [28]. The 3D reciprocal space map have been visualized finally using the ParaView software.

### High-resolution transmission electron microscopy

HR-TEM investigations were performed with $[1\bar{1}0]$ zone axis at an accelerating voltage of 300 kV on a JEOL JEM-3010 instrument with a spatial resolution of 0.17 nm. Using focused ion beam preparation procedure (Dual beam FIB, FEI Helios 600 NanoLab), electron transparent ultra-thin sections were extracted from the thin films of GeTe on Si. The typical dimensions of the electron transparent ultrathin sections are 15 $\mu$m (length) × 5 $\mu$m (height) × 150–200 nm (thickness). GPA analysis was performed using the strain++ software applying a mask in reciprocal space of radius 0.8 $nm^{-1}$ producing a lateral resolution in the images of 1.25 nm.

### Second Harmonic Generation microscopy and polarimetry analysis

Local second harmonic generation (SHG) measurements were conducted by means of an inverted optical microscope. The fundamental wave is provided by a laser source emitting pulses of 100 fs duration at a repetition rate of 80 MHz, centered at a wavelength $\lambda$ = 800 nm. The sample was illuminated at normal incidence with a time-averaged power of 11 mW. The SHG images are obtained by scanning the sample with respect to the focused laser beam (objective ×60, 0.85 numerical aperture (NA)) using computer-controlled stepping motors. The output intensity was spectrally filtered and collected into a photomultiplier. Polarimetry measurements are performed by recording the SHG images at different polarizer and analyzer angles. In the case of a a medium focusing of the fundamental beam (0.70 NA, or smaller), a scalar model using the analytic form of SHG is sufficient to model the local polarimetry response at polar domains [29], domain walls.[30–32] The use of a strong focusing (0.85 NA ) was necessary in this study to properly resolve the fine ferroelastic needles. In this case a vectorial treatment of the fundamental electric field is necessary [33]. We have thus developed a semi-analytic model for the second harmonic polarimetry, combining the analytic form of SHG with a vectorial modelling of the fundamen-

tal focused electric field. The as derived fitting functions take also into account the mixed character of the studied volumes (containing both a- and c-domain fractions) in both polarization plots (P-plots) and anisotropy plots (simultaneous rotation of the polarization and analyzer). The fitting functions related to both measurement geometries are presented in the Supplementary Note 1.

## III. RESULTS AND DISCUSSION

In order to determine the structure of GeTe thin films we have performed X-ray diffraction measurements. In Figure 1a, the iso-intensity surfaces of 3D reciprocal space maps [34] of GeTe epitaxial thin films close to $222_c$ show four Bragg peaks ($c$ stands for a pseudocubic unit cell). The main Bragg peak is located along the axis perpendicular to the surface and is centered at $q_z$=35.408 nm$^{-1}\pm$ 0.010 nm$^{-1}$. This Bragg peak position at low $q_z$ can be assigned to a rhombohedral distortion of GeTe thin films stretched along the [111] growth axis. In the following the real space regions giving rise to this Bragg peak are referred as $c$-domains that constitute the vast majority of the thin film. In addition three minor Bragg peaks are slightly angularly offset from this axis and localized at higher $q_z$=36.733 nm$^{-1}\pm$ 0.010 nm$^{-1}$. They can be assigned to minor ferroelastic domains with a rhombohedral distortion along [11$\bar{1}$], [1$\bar{1}$1] and [$\bar{1}$11] (labelled $a$-domains). These distortions induce a rotation of the (111) crystallographic planes by $1.36^\circ \pm 0.04^\circ$ (see Figure 1a-(iii)) and a slight compression of the (111) inter-reticular distance of 3.74% with respect to $c$-domains.

To determine the domain boundary type, the X-ray diffuse scattering around Bragg peaks provides some hints. The minor Bragg peaks from the ferroelastic $a$-domains are clearly elongated along a precise direction in reciprocal space ($37^\circ \pm 3^\circ$ with respect to $q_z$ axis) and this extension is more pronounced for thinner films (60 nm-thick GeTe thin film). This diffuse scattering indicates the presence of well defined interfaces between $a$- and $c$-domains and can be assigned to 71°-type domain walls due to finite size effect along the [110] direction (Figure 1c). TEM cross-section views (Figure 1b) show indeed that ferroelastic $a$-domains are crossing the film with sharp and straight walls perpendicular to the [110] direction. These sharp interfaces are the only one observed between the $c$-domains and $a$-domains. For the thinnest films (Figure 1a-(i)), no additional X-ray diffuse scattering is measured indicating that ferroelastic $a$-domains are independent and do not intersect each other. For thicker films, the volume fraction of ferroelastic $a$-domains increases as shown by the increase of the ratio of the integrated intensities of minor Bragg peaks with respect to the major peak (Figure 1d). This gives rise also to a more complex diffuse scattering pattern originating from the intersection area between ferroelastic $a$-domains of different variants. Experimental signatures of these intersections arise from diffuse scattering bridge patterns [34 and 35] localized between ferroelastic $a$-nanodomain Bragg peaks (Figure 1a-(iii)). The center of mass of the bridges indicates a 60° in-plane rotation of the strain, a tilt angle of $0.79^\circ \pm 0.05^\circ$ and an increased compression of the (111) crystallographic planes by 4.37% in the intersection area ($q_z$=36.954 nm$^{-1}\pm$ 0.010 nm$^{-1}$). Complementary X-ray diffraction measurements on non-symmetric Bragg peaks show that all the domains have a rhombohedral structure (a=0.429 nm, $\alpha$=58.3°) and that a single epitaxy exists with the Si substrate such that $\alpha$-GeTe(111)$\|$Si(111) and $\alpha$-GeTe[1$\bar{1}$0]$\|$Si[1$\bar{1}$0] [23] in pseudocubic coordinates. We can also estimate the average azimuthal misorientation between grains to be $0.7^\circ \pm 0.2^\circ$ (Supplementary materials S1). Moreover, as shown from the threefold symmetry of the $222_c$ Bragg peaks, the fraction of twinned grains is negligible in the layer. We estimate from the intensity of Bragg peaks that less than 5% of the layer contains twinned grains (less than 10% for the 60 nm-thick GeTe film).

In addition to the rhombohedral distortion of the GeTe unit cell, SHG microscopy combined to polarimetry analysis is a highly suited method to investigate the local symmetry and obtain the domain structure of non-centrosymmetric ferroic materials. This method is applied here to obtain the detailed domain structure of a thick GeTe film. Figure 2a shows a SHG image of a thick GeTe film revealing stripe domains superimposed to a background exhibiting a lower emission intensity. This image regroups all the domain contributions by combining three SHG images recorded at different sets of polarizer and analyser angles as explained in the Supplementary Figure S2. The observation of the fine ferroelastic stripes is made possible by a convolution mechanism in SHG microscopy involving the focused laser (Gaussian) beam and the comparatively zero-size of the nano-object like in the SHG imaging of domain walls.[32] This artificial broadening allows for the observation of the nanoscale domains and the spectral analysis of the their local emission (see Supplementary Figure S3). The local polarization is derived through the precise modeling of the local SHG polarimetry (see methods) and the result is displayed in the inset of Figure 2a. The GeTe(111) films show three domain stripes oriented in-plane at 0° and ± 120° with a polarization oriented along the width of the stripes (see more details in Supplementary Figures S4-S6). The local SHG polarimetry confirms also the 3m point group symmetry of the film and reveals a background showing out-of-plane polarization.

As these ferroelastic nanodomains meet the surface of the film they can be characterised by surface sensitive techniques, such as low energy electron microscopy (LEEM), with much higher resolution [36] (see Figure 2b-c). The LEEM contrast in reflectivity mode (bright field) shows bright and dark bands of intensity along the domains that reverse with the focusing conditions of the microscope [37] (See supplementary materials S7). This is typical feature of a ridge-and-valley morphology

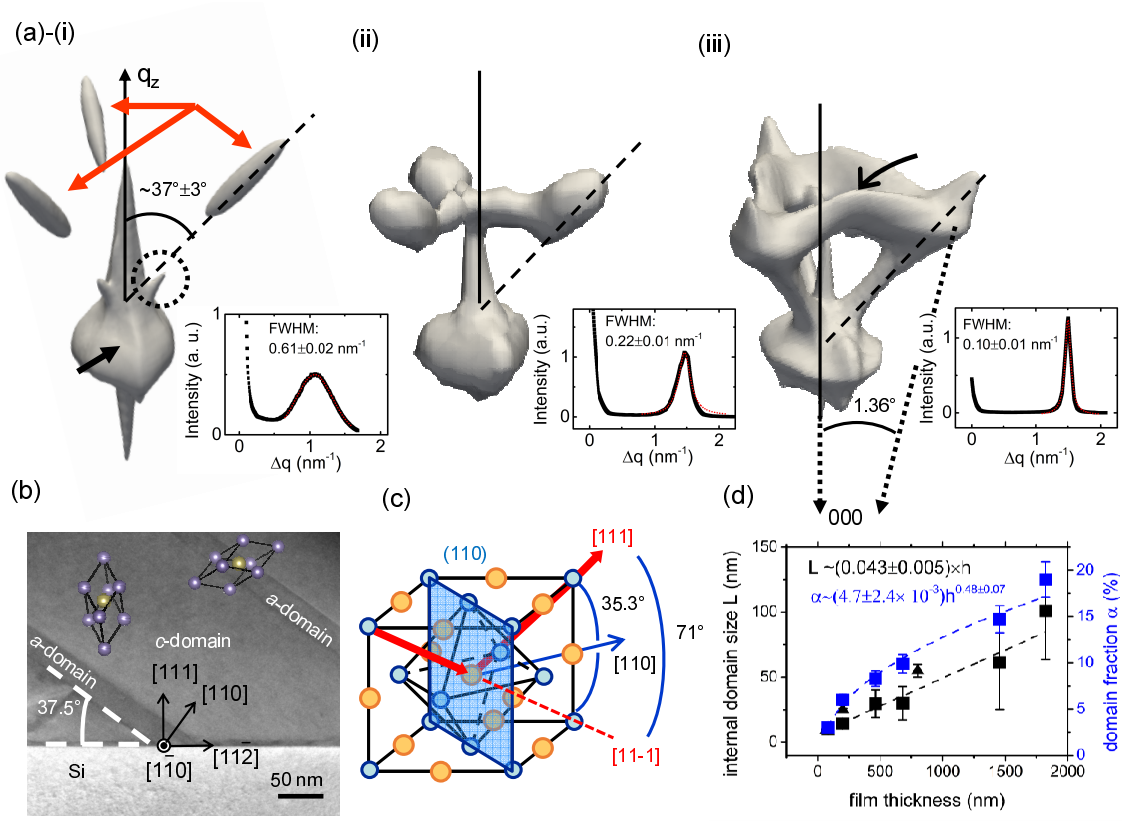


FIG. 1. (a)-(i) iso-intensity surface (2500 counts) of a 3D reciprocal space map around $222_c$ Bragg peak of a 60 nm-thick GeTe thin film. Bragg peaks of main GeTe $c$-domains (black arrow) and ferroelastic $a$-nanodomains (red arrows). Minor ferroelastic Bragg peaks from the $a$-nanodomains are elongated at $\sim 37° \pm 3°$ with respect to $q_z$ axis (line profile along the dashed line in inset). Similar elongation of the diffuse scattering of GeTe $c$-domain (dotted circle) arising from the truncation of the $c$-domains by inclined $a$-domains (Babinet principle). (ii) and (iii) Same as (i) for a 200 nm (5000 counts) and 800 nm-thick (3000 counts) GeTe thin film. X-ray diffuse scattering bridge due to domains intersection (curved black arrow). (b) TEM cross-section of a 460 nm-thick GeTe thin film with medium resolution showing 2 $a$-nanodomains crossing the film ($[1\bar{1}0]$ zone axis). The rhombohedral unit cells indicates the elongation direction of the domains. (c) Scheme of the polarization (rhombohedral elongation) of the main GeTe $c$-domains along [111] and a secondary ferroelastic $a$-domain along $[11\bar{1}]$ (in pseudocubic representation). (d) Domain size L and volume fraction $\alpha$ of ferroelastic domains in GeTe thin films as function of film thickness deduced from the full width at half maximum of diffraction peaks of ferroelastic domains (triangle) and LEEM measurements (square).

and that indicates that the surface of the nanodomains is tilted. Tilted surface patterns are characteristic features of ferroelastic domains. The mean tilt angle of the nanodomains has been quantitatively characterized by $\mu$-LEED [38]. The reflected beams from the three domains variants ($0$ ,$\pm$ 120°) are slightly off-specular with respect to the main (0,0) reflected beam (Figure 2d and inset of Figure 2e) and the angular shift increases with the incident electron energy $E$ (Figure 2e). Quantitatively the triangle area $A$ formed by the 3 equivalent reflected beams increases as:

$$A = \frac{18}{\sqrt{3}} \frac{m}{\hbar^2} \pi \theta^2 E \qquad (1)$$

where $\theta$ is the tilt angle ($\theta \ll 1$), $m$ is the electron mass and $\hbar$ is the reduced Planck constant. These domains have a mean surface plane orientation that is tilted by $1.37° \pm 0.03°$ in the $\langle 11\bar{2} \rangle$ direction with respect to the average surface plane. These tilted planes make the same tilt angle as the (111) crystallographic planes of the $a$-nanodomains obtained from the position of the minor Bragg peaks measured by X-ray diffraction. This unambiguously confirms the same ferroelastic origin of the nanodomains at the surface and in the bulk of the layer. From LEEM topographic measurements we have also quantified the evolution of the $a$-domain fraction $\alpha$ as a function of the film thickness (Figure 1d). Below 30 nm, the $a$-domain fraction is null and the film is therefore monodomain. Then it increases sub-linearly [10 and 39] as $\alpha \sim [4.7 \pm 2.4] \times 10^{-3} h^{0.48 \pm 0.07}$ ($h$ is the film thickness in nm). The domain width $L$ (Figure 1d) increases linearly over the entire range of thickness as $L \sim [0.043 \pm 0.005] h$ nm and reaches $\sim$ 77 nm for a 1825

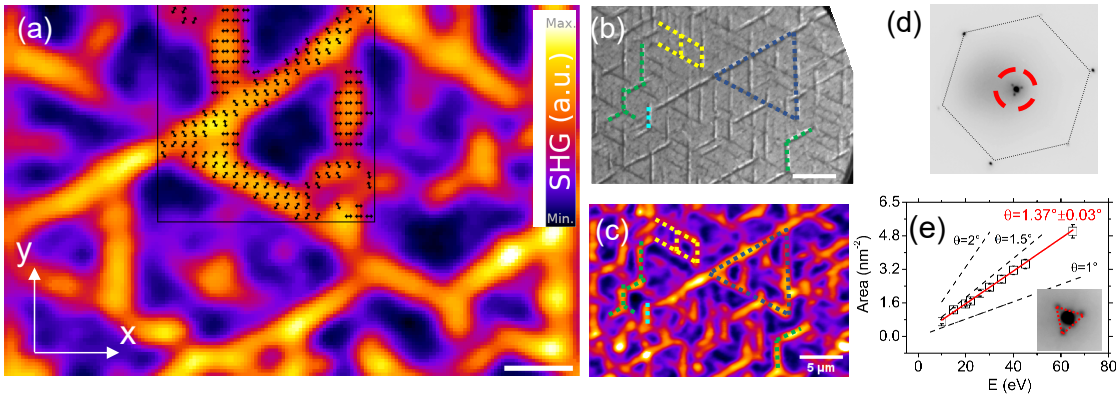


FIG. 2. (a) Isotropic second harmonic image revealing the domain structure of a 1825 nm-thick GeTe film. The black arrows indicate the local in-plane polarization orientation in the nanodomains as derived from pixel-by-pixel polarimetry analysis (see Supplementary Figure S3). The three different $a$-domain contributions (at $-30°$, $30°$ and $90°$ with respect to $x$ axis) are superimposed to the background (dark purple) signal exhibiting out-of-plane polarisation ($c$-domain). The scale bar corresponds to 2 $\mu$m. (b) LEEM image (bright field mode, incident electron energy: 26 eV) from the GeTe thin film (scale bar 5 $\mu$m). (c) Same area visualized by spatially resolved SHG. Dashed lines in (b) and (c) are markers. (d) $\mu$-LEED pattern (20 $\mu$m incident beam size) at 26 eV incident electron energy showing 4 reflected beams inside red dot circle: a main reflected beam and three minor beams originating from the nanodomains.(e) Area of the triangle formed by the three reflected beams (nanodomains) as function of the incident electron energy (from 8 to 65 eV). Linear fit (red line) and simulations for different tilt angles (dashed lines).

nm-thick GeTe film. These LEEM measurements are also confirmed with the estimate of the $a$-nanodomain size from the full width at half maximum of the diffraction peaks of the minor domains (insets in figure 1a). The domain fraction and domain size results allow to evaluate the effective period $W = L/\alpha$ of the nanodomain pattern. It reaches ~500 nm for a 1825 nm-thick GeTe film. Assuming in the mean strain approach [40–42] that:

$$W = \frac{\sqrt{h_0 h}}{2\xi\alpha\,(1-\alpha)} \qquad (2)$$

with $\xi = 0.27$, we have estimated a characteristic length $h_0 = 0.5 \pm 0.2$ nm of the nanodomain pattern that balances the gain of elastic energy and the costs of domain wall and interfacial stress with the substrate.

The atomic scale characterization of the 71°-type domain walls and $a$-domains has been addressed by high-resolution transmission electron microscopy (HR-TEM [43]). Figure 3a shows an area including the Si substrate, a $a$-domain and a $c$-domain separated by a 71°-type domain wall. Strain and rotation mapping of the crystalline lattice of the GeTe layer in this area can be determined by comparison with a reference (unstrained) region of the Si substrate far from the interface. This has been carried out using the image-processing technique called the geometric phase analysis (GPA) [5, 44, and 45]. Considering that the $x$ and $y$ axes are respectively parallel and perpendicular to the domain wall, we evidence that the diagonal components of the strain tensor, $\epsilon_{xx}$ and $\epsilon_{yy}$, are equal on both sides of the wall whereas the pure shear component $\epsilon_{xy}$ and rotation field $\omega_{xy}$ make a significant jump across the domain wall (figure 3b). One can notice that shear and rotation (2.2°) components compensate across the wall to have a coplanar (110) plane as expected from mechanical compatibility of the interface between $a$- and $c$-domains (figure 3c) [46].

Ferroelastic nanodomain formation and ferroelectric switching processes are known to be highly sensitive to the mechanical interactions with the substrate due to the stress induced by the lattice mismatch. This effect may be even more pronounced for epitaxial films. To address the relaxation mechanisms prevailing in the formation of these ferroelastic nanodomains we have characterized the GeTe/Si interface with HR-TEM. Figure 4a shows the in-plane strain field ($\epsilon_{xx}$) across the interface with $x$ along $\langle 11\bar{2}\rangle$. The lattice parameter mismatch between the Si substrate and the GeTe $c$-domain is locally 8.2±0.2% (figure 4c). In the $a$-nanodomain $\epsilon_{xx}$ is larger (12.2±0.2%) due to the nearly in-plane stretch of the rhombohedral distortion. Considering the lattice mismatch the formation of $a$-domains is elastically unfavorable if the in-plane lattice deformation is fixed by the Si substrate lattice parameter. However the regular modulation of the in-plane strain component $\epsilon_{xx}$ in GPA analysis shows that this huge lattice parameter mismatch between the Si substrate and GeTe thin film is relaxed *via* interfacial misfit dislocations with a period of 4.10 nm (resp. 2.77 nm) for the $c$-domain (resp. $a$-domain). This result shows that the dislocation-assisted stress release is the main relaxation mechanism of the interface (see figure 4b). To compare the interfacial energy cost of both GeTe $c$-domains and $a$-domains we can make some preliminary remarks. (i) The linear density of misfit dislocations is higher for the $a$-domains (0.36 nm$^{-1}$) than for the $c$-domains (0.24 nm$^{-1}$). (ii) The in-plane lattice of the $a$-nanodomains

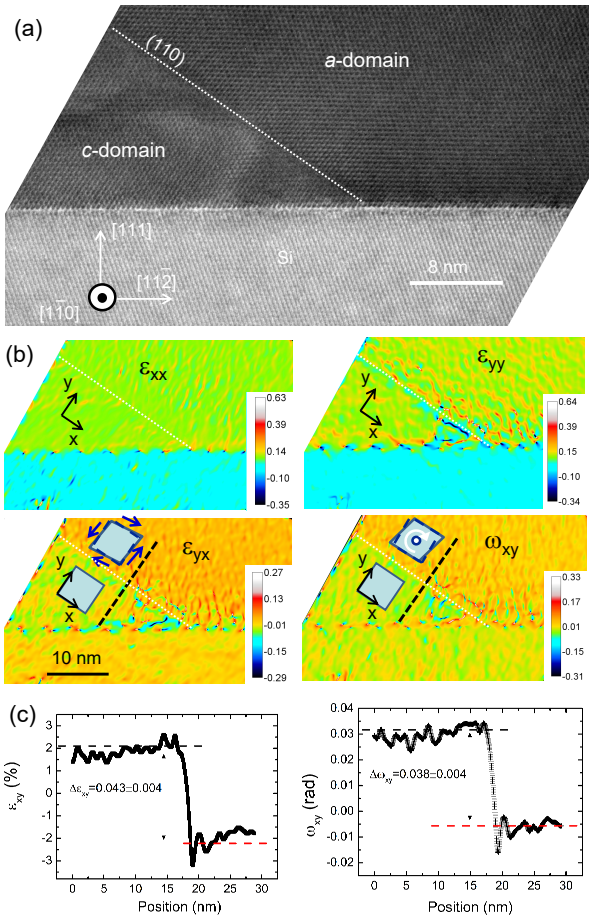


FIG. 3. (a) HR-TEM cross-section ($\langle 1\bar{1}0\rangle$ zone axis) of the interfacial area between the Si substrate, a GeTe $c$-domain and a $a$-nanodomain (domain wall: dotted white line) for a 460 nm-thick GeTe film. (b) In-plane $\epsilon_{xx}$, out-of-plane $\epsilon_{yy}$, shear $\epsilon_{xy}$ strain and rotation $\omega_{xy}$ with $x$ and $y$ respectively parallel and perpendicular to the domain wall. (c) Line profiles of shear and rotation across the wall (see dark dashed-line in (b)).

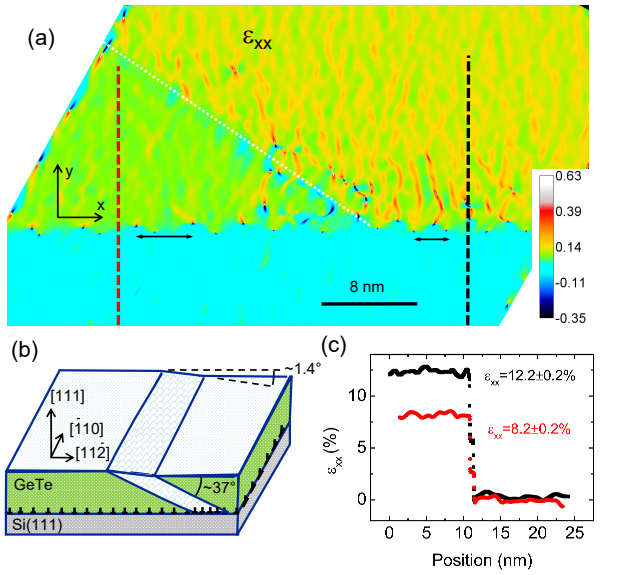


FIG. 4. (a) In-plane strain $\epsilon_{xx}$ with $x$ along the $\langle 11\bar{2}\rangle$ GeTe/Si interface obtained from GPA analysis. The arrows at the GeTe/Si interface show the regular modulation of $\epsilon_{xx}$. (b) Model of the internal structure of GeTe thin films on Si(111). (c) Line profiles of in-plane strain $\epsilon_{xx}$ across the interface (see dashed line in (a): dark (resp. red) line across the $a$-domain (resp. $c$-domain).

is monoclinic whereas it is hexagonal for the GeTe $c$-domains (as for the Si substrate). (iii) At last the interface plane of the $a$-nanodomains is expected to be tilted by 1.36° with respect to the Si surface plane (tilt angle of (111) plane) whereas the main GeTe $c$-domain and Si substrate are coplanar. Therefore the formation of the $a$-nanodomains appears to be energetically unfavorable.

To address the metastability of these $a$-nanodomains we have performed LEEM measurements during heating and cooling thermal treatments of GeTe thin films (see Supplementary Figure S8 and corresponding movie). Figure 5 shows that the ferroelastic nanodomains disappear at ∼250° C, *i.e.* slightly below the thin film growth temperature (275 ° C) and far below the Curie temperature (∼ 400° C). Therefore we assume that a ferroelastic configuration with only a single domain occurs during GeTe growth with a unique rhombohedral distortion perpendicular to the film. When cooling, the ferroelastic $a$-nanodomains nucleate abruptly at 210±10° C. This process is perfectly reproducible cycling the temperature. To explain this behaviour we infer that upon cooling a thermal stress arises due to the different linear thermal expansion coefficients of GeTe [47 and 48] $\sim 31.9\times10^{-6}$ $K^{-1}$ and Si [49 and 50] $\sim 3.5\times10^{-6}$ $K^{-1}$. Assuming that the interfacial misfit dislocations are not enough mobile to accommodate this change [51–54] and given that GeTe lattice parameter should decrease faster than that of Si substrate, a tensile in-plane strain occurs in the GeTe layer. A very efficient way to macroscopically reduce this stress is to nucleate $a$-domains that expand locally the in-plane lattice parameter in the $\langle 11\bar{2}\rangle$ direction. The three variants of the ferroelastic domains provides a global isotropic relaxation. When the GeTe layer is annealed at a temperature close to the growth temperature it recovers its growth lattice parameter, and therefore the $a$-nanodomains are elastically useless and spontaneously decay (see Figure 5b-c). The hysteretic behaviour of the $a$-domains indicates also that a nucleation energy barrier must be overpassed for their formation.

## IV. CONCLUSION

In conclusion the domain structure of $\alpha$-GeTe thin films epitaxially grown on Si(111) has been investigated. By combining 3D reciprocal space mapping by X-ray

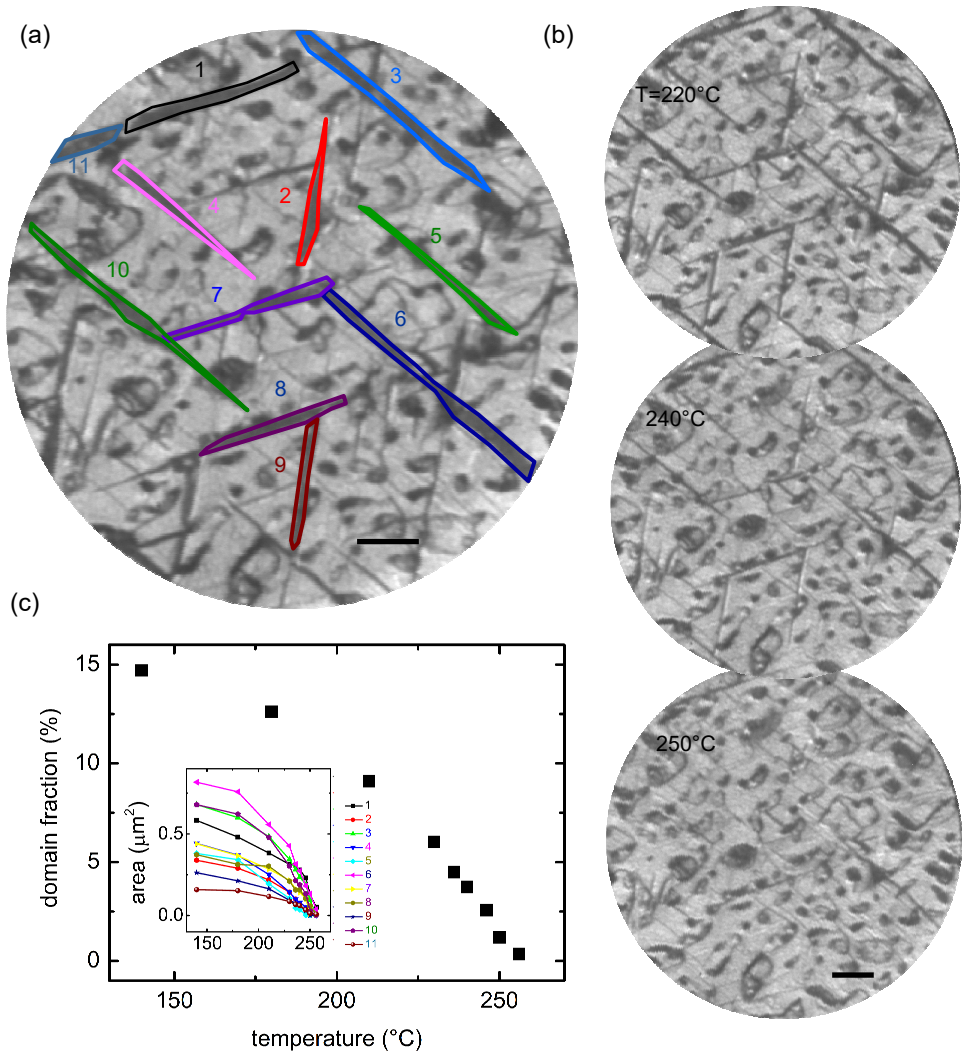


FIG. 5. (a) LEEM image (bright-field mode excluding the reflected beam from the nanodomains) of GeTe thin film (1455 nm) at 180° C. (b) Series of LEEM images at 220, 240 and 250° C. Scale bar 1 $\mu$m. (c) Temperature evolution of $a$-nanodomains fraction as function of temperature (inset: temperature evolution of some domains area shown in (a)). The dark contrast areas that have not a needle shape correspond to local depressions in the GeTe thin film.

diffraction, HR-TEM, SHG and LEEM we have quantified the volume fraction and size of the nanodomains as function of the film thickness. We have demonstrated that domain walls are only of 71°-type and the interface with the Si substrate is stabilized by misfit dislocations that relaxes the large lattice parameter mismatch. Using *in situ* LEEM under cooling we have shown that the ferroelectric $a$-nanodomains nucleate and grow whereas they decay under annealing and disappear at 250 °C. This result indicates that during GeTe growth at 275 °C, a single domain configuration occurs with a polarization perpendicular to the film surface. We infer that this single domain state during growth is a key parameter that favors the high crystalline quality of the GeTe layer. Then the driving force for the formation of the ferroelectric nanodomains at lower temperature is attributed to the thermal stress as the dislocations are frozen and cannot accommodate the relative change of lattice parameter. We believe that this detailed description of domain behavior as a function of temperature and film thickness will serve as a playground for the control of ferroelectric/ferroelastic nanodomains in GeTe and will motivate new strategies to tune the Rashba effect by addressing the motion of domain walls.

## Supporting Information

Supporting Information is available from the Online Library or from the author.

## Acknowledgements

The project leading to this publication has received funding from Excellence Initiative of Aix-Marseille University A*MIDEX, a french "Investissements d'Avenir" programme through the AMUtech Institute. This work has also been supported by the ANR grants HOLOLEEM

(ANR-15-CE09-0012) and TOPELEC (ANR-18-CE92-0052). S.C.-H. and C.V. acknowledge funding by the LabEx NIE (ANR-11-LABX-0058-NIE) in the framework of the Interdisciplinary Thematic Institute QMat (ANR-17-EURE-0024), as part of the ITI 2021-2028 program supported by the IdEx Unistra (ANR-10-IDEX-0002-002) and SFRI STRATUS (ANR-20-SFRI-0012) through the French Programme d'Investissement d'Avenir. The authors acknowledge the assistance of O. Grégut during SHG measurements and insightful discussion about symmetry aspects with U. Acevedo-Salas. We are grateful to Martiane Cabié (CP2M, Marseille) for lamella preparation of GeTe thin films by Focused Ion Beam.

[1] N. A. Pertsev, A. G. Zembilgotov, and A. K. Tagantsev. Effect of Mechanical Boundary Conditions on Phase Diagrams of Epitaxial Ferroelectric Thin Films. *Physical Review Letters*, 80(9):1988–1991, 1998.

[2] M. Dawber, K. M. Rabe, and J. F. Scott. Physics of thin-film ferroelectric oxides. *Reviews of Modern Physics*, 77(4):1083–1130, 2005.

[3] J. M. Gregg. Ferroelectrics at the nanoscale. *physica status solidi (a)*, 206(4):577–587, 2009.

[4] G. Catalan, A. Janssens, G. Rispens, S. Csiszar, O. Seeck, G. Rijnders, D. H. A. Blank, and B. Noheda. Polar Domains in Lead Titanate Films under Tensile Strain. *Physical Review Letters*, 96(12):127602, 2006.

[5] G. Catalan, A. Lubk, A. H. G. Vlooswijk, E. Snoeck, C. Magen, A. Janssens, G. Rispens, G. Rijnders, D. H. A. Blank, and B. Noheda. Flexoelectric rotation of polarization in ferroelectric thin films. *Nature Materials*, 10(12):963–967, 2011.

[6] Tomoaki Yamada, Daisuke Ito, Tomas Sluka, Osami Sakata, Hidenori Tanaka, Hiroshi Funakubo, Takahiro Namazu, Naoki Wakiya, Masahito Yoshino, Takanori Nagasaki, and Nava Setter. Charge screening strategy for domain pattern control in nano-scale ferroelectric systems. *Scientific Reports*, 7(1):5236, 2017.

[7] A. K. Yadav, C. T. Nelson, S. L. Hsu, Z. Hong, J. D. Clarkson, C. M. Schlepueetz, A. R. Damodaran, P. Shafer, E. Arenholz, L. R. Dedon, D. Chen, A. Vishwanath, A. M. Minor, L. Q. Chen, J. F. Scott, L. W. Martin, and R. Ramesh. Observation of polar vortices in oxide superlattices. *Nature*, 530(7589):198+, 2016.

[8] Marios Hadjimichael, Yaqi Li, Edoardo Zatterin, Gilbert A Chahine, Michele Conroy, Kalani Moore, Eoghan N O' Connell, Petr Ondrejkovic, Pavel Marton, Jiri Hlinka, Ursel Bangert, Steven Leake, and Pavlo Zubko. Metal–ferroelectric supercrystals with periodically curved metallic layers. *Nature Materials*, 20(4):495–502, 2021.

[9] Ekhard K. H. Salje. Ferroelastic domain walls as templates for multiferroic devices. *Journal of Applied Physics*, 128(16):164104, 2020.

[10] V Nagarajan, IG Jenkins, SP Alpay, H Li, S Aggarwal, L Salamanca-Riba, AL Roytburd, and R Ramesh. Thickness dependence of structural and electrical properties in epitaxial lead zirconate titanate films. *Journal of Applied Physics*, 86(1):595–602, 1999.

[11] A. H.G. Vlooswijk, B. Noheda, G. Catalan, A. Janssens, B. Barcones, G. Rijnders, D. H.A. Blank, S. Venkatesan, B. Kooi, and J. T.M. De Hosson. Smallest 90° domains in epitaxial ferroelectric films. *Applied Physics Letters*, 91(11):20–23, 2007.

[12] L. Feigl, L. J. McGilly, C. S. Sandu, and N. Setter. Compliant ferroelastic domains in epitaxial Pb(Zr,Ti)O 3 thin films. *Applied Physics Letters*, 104(17):172904, 2014.

[13] Domenico Di Sante, Paolo Barone, Riccardo Bertacco, and Silvia Picozzi. Electric Control of the Giant Rashba Effect in Bulk GeTe. *Advanced Materials*, 25(4):509–513, 2013.

[14] Marcus Liebmann, Christian Rinaldi, Domenico Di Sante, Jens Kellner, Christian Pauly, Rui Ning Wang, Jos Emiel Boschker, Alessandro Giussani, Stefano Bertoli, Matteo Cantoni, Lorenzo Baldrati, Marco Asa, Ivana Vobornik, Giancarlo Panaccione, Dmitry Marchenko, Jaime Sanchez-Barriga, Oliver Rader, Raffaella Calarco, Silvia Picozzi, Riccardo Bertacco, and Markus Morgenstern. Giant Rashba-Type Spin Splitting in Ferroelectric GeTe(111). *Advanced Materials*, 28(3):560+, 2016.

[15] Christian Rinaldi, Sara Varotto, Marco Asa, Jagoda Slawinska, Jun Fujii, Giovanni Vinai, Stefano Cecchi, Domenico Di Sante, Raffaella Calarco, Ivana Vobornik, Giancarlo Panaccione, Silvia Picozzi, and Riccardo Bertacco. Ferroelectric Control of the Spin Texture in GeTe. *Nano Letters*, 18(5):2751–2758, 2018.

[16] J. Krempasky, S. Muff, J. Minar, N. Pilet, M. Fanciulli, A. P. Weber, E. B. Guedes, M. Caputo, E. Mueller, V. V. Volobuev, M. Gmitra, C. A. F. Vaz, V Scagnoli, G. Springholz, and J. H. Dil. Operando Imaging of All-Electric Spin Texture Manipulation in Ferroelectric and Multiferroic Rashba Semiconductors. *Physical Review X*, 8(2), 2018.

[17] C. Rinaldi, J. C. Rojas-Sanchez, R. N. Wang, Y. Fu, S. Oyarzun, L. Vila, S. Bertoli, M. Asa, L. Baldrati, M. Cantoni, J. M. George, R. Calarco, A. Fert, and R. Bertacco. Evidence for spin to charge conversion in GeTe(111). *APL Materials*, 4(3), 2016.

[18] Jagoda Slawinska, Domenico Di Sante, Sara Varotto, Christian Rinaldi, Riccardo Bertacco, and Silvia Picozzi. Fe/GeTe(111) heterostructures as an avenue towards spintronics based on ferroelectric Rashba semiconductors. *Physical Review B*, 99(7), 2019.

[19] Yan Li, Yang Li, Peng Li, Bin Fang, Xu Yang, Yan Wen, Dong-xing Zheng, Chen-hui Zhang, Xin He, Aurelien Manchon, Zhao-Hua Cheng, and Xi-xiang Zhang. Nonreciprocal charge transport up to room temperature in bulk Rashba semiconductor alpha-GeTe. *Nature Communications*, 12(1), 2021.

[20] Ho Seong Lee, Bong-Seo Kim, Chang-Woo Cho, Min-Wook Oh, Bok-Ki Min, Su-Dong Park, and Hee-Woong Lee. Herringbone structure in GeTe-based thermoelectric materials. *Acta Materiala*, 91:83–90, 2015.

[21] Paul A. Vermeulen, Anil Kumar, Gert H. ten Brink, Graeme R. Blake, and Bart J. Kooi. Unravelling the Domain Structures in GeTe and LaAlO3. *Crystal Growth & Design*, 16(10):5915–5922, 2016.

[22] A. V. Kolobov, D. J. Kim, A. Giussani, P. Fons, J. Tominaga, R. Calarco, and A. Gruverman. Ferroelectric switching in epitaxial GeTe films. *APL Materials*, 2(6), 2014.

[23] Ruining Wang, Jos E. Boschker, Emilie Bruyer, Domenico Di Sante, Silvia Picozzi, Karthick Perumal, Alessandro Giussani, Henning Riechert, and Raffaella Calarco. Toward Truly Single Crystalline GeTe Films: The Relevance of the Substrate Surface. *Journal of Physical Chemistry C*, 118(51):29724–29730, 2014.

[24] Dominik Kriegner, Gunther Springholz, Carsten Richter, Nicolas Filet, Elisabeth Mueller, Marie Capron, Helmut Berger, Vaclay Holy, J. Hugo Dil, and Juraj Krempasky. Ferroelectric Self-Poling in GeTe Films and Crystals. *Crystals*, 9(7), 2019.

[25] Silvia Picozzi. Ferroelectric Rashba semiconductors as a novel class of multifunctional materials. *Frontiers in Physics*, 2:10, 2014.

[26] Silvia Picozzi. *Multiferroic and Ferroelectric Rashba Semiconductors*, pages 375–400. Springer International Publishing, Cham, 2020.

[27] S Andrieu. Sb adsorption on Si(111) analyzed by ellipsometry and reflection high energy electron diffraction: Consequences for Sb doping in Si molecular beam epitaxy. *Journal of Applied Physics*, 69(3):1366–1370, 1991.

[28] Cristian Mocuta, Marie-Ingrid Richard, Julie Fouet, Stefan Stanescu, Antoine Barbier, Christophe Guichet, Olivier Thomas, Stephanie Hustache, Alexey V. Zozulya, and Dominique Thiaudiere. Fast pole figure acquisition using area detectors at the DiffAbs beamline - Synchrotron SOLEIL. *Journal of Applied Crystallography*, 46(6):1842–1853, DEC 2013.

[29] Sava A. Denev, Tom T.A. Lummen, Eftihia Barnes, Amit Kumar, and Venkatraman Gopalan. Probing ferroelectrics using optical second harmonic generation. *Journal of the American Ceramic Society*, 94(9):2699–2727, 2011.

[30] Salia Cherifi-Hertel, Herve Bulou, Riccardo Hertel, Gregory Taupier, Kokou Dodzi (Honorat) Dorkenoo, Christian Andreas, Jill Guyonnet, Iaroslav Gaponenko, Katia Gallo, and Patrycja Paruch. Non-Ising and chiral ferroelectric domain walls revealed by nonlinear optical microscopy. *Nature Communications*, 8, 2017.

[31] Hiroko Yokota and Yoshiaki Uesu. Optical second-harmonic generation microscopy as a tool for ferroelastic domain wall exploration. *Journal of Applied Physics*, 129(1):014101, 2021.

[32] Salia Cherifi-Hertel, Cédric Voulot, Ulises Acevedo-Salas, Yide Zhang, Olivier Crégut, Kokou Dodzi Dorkenoo, and Riccardo Hertel. Shedding light on non-Ising polar domain walls: Insight from second harmonic generation microscopy and polarimetry analysis. *Journal of Applied Physics*, 129(8):081101, 2021.

[33] K. J. Spychala, P. Mackwitz, A. Widhalm, G. Berth, and A. Zrenner. Spatially resolved light field analysis of the second-harmonic signal of $\chi(2)$-materials in the tight focusing regime. *Journal of Applied Physics*, 127(2), 2020.

[34] Z. L. Luo, H. Huang, H. Zhou, Z. H. Chen, Y. Yang, L. Wu, C. Zhu, H. Wang, M. Yang, S. Hu, H. Wen, X. Zhang, Z. Zhang, L. Chen, D. D. Fong, and C. Gao. Probing the domain structure of BiFeO3 epitaxial films with three-dimensional reciprocal space mapping. *Applied Physics Letters*, 104(18), 2014.

[35] J Chrosch and EKH Salje. Temperature dependence of the domain wall width in LaAlO3. *Journal of Applied Physics*, 85(2):722–727, 1999.

[36] N. Barrett, J. E. Rault, J. L. Wang, C. Mathieu, A. Locatelli, T. O. Mentes, M. A. Niño, S. Fusil, M. Bibes, A. Barthélémy, D. Sando, W. Ren, S. Prosandeev, L. Bellaiche, B. Vilquin, A. Petraru, I. P. Krug, and C. M. Schneider. Full field electron spectromicroscopy applied to ferroelectric materials. *Journal of Applied Physics*, 113(18):187217, 2013.

[37] K. M. Yu, A. Locatelli, and M. S. Altman. Comparing Fourier optics and contrast transfer function modeling of image formation in low energy electron microscopy. *Ultramicroscopy*, 183:109–116, DEC 2017. 10th International Workshop on Low Energy Electron Microscopy and Photoemission Electron Microscopy (LEEM/PEEM), Monterey, CA, SEP 11-15, 2016.

[38] WX Tang, KL Man, HC Huang, CH Woo, and MS Altman. Growth shapes of Ag crystallites on the Si(111) surface. *Journal of Vacuum Science & Technology B*, 20(6):2492–2495, NOV-DEC 2002. 3rd Low Energy Electron Microscopy/Photoemission Electron Microscopy Workshop, Albuquerque, NM, MAY 14-17, 2002.

[39] WY Hsu and R Raj. X-ray characterization of the domain-structure of epitaxial Lead Titanate thin-films on (001)-Strontium Titanate. *Applied Physics Letters*, 67(6):792–794, 1995.

[40] AL Roytburd. Thermodynamics of polydomain heterostructures. I. Effect of macrostresses. *Journal of Applied Physics*, 83(1):228–238, 1998.

[41] AL Roytburd. Thermodynamics of polydomain heterostructures. II. Effect of microstresses. *Journal of Applied Physics*, 83(1):239–245, 1998.

[42] AK Tagantsev, LE Cross, and J Fousek. Domains in Ferroic Crystals and Thin Films. In *Domains in Ferroic Crystals and Thin Films*, pages 1–821. 2010.

[43] Etienne Snoeck, Axel Lubk, and César Magén. *Structural Characterization of Ferroelectric and Multiferroic Nanostructures by Advanced TEM Techniques*, chapter 10, pages 275–324. John Wiley & Sons, Ltd, 2016.

[44] MJ Hytch, E Snoeck, and R Kilaas. Quantitative measurement of displacement and strain fields from HREM micrographs. *Ultramicroscopy*, 74(3):131–146, 1998.

[45] JL Rouviere and E Sarigiannidou. Theoretical discussions on the geometrical phase analysis. *Ultramicroscopy*, 106(1):1–17, 2005.

[46] Jan Fousek and Vaclav Janovec. The Orientation of Domain Walls in Twinned Ferroelectric Crystals . *Journal of Applied Physics*, 40:135–142, 1969.

[47] T Chattopadhyay, JX Boucherle, and HG Vonschnering. Neutron diffraction study on the structural phase transition in GeTe. *Journal of Physics C: Solid State Physics*, 20(10):1431–1440, 1987.

[48] Marion Gallard, Mohamed Salah Amara, Magali Putero, Nelly Burle, Christophe Guichet, Stephanie Escoubas, Marie-Ingrid Richard, Cristian Mocuta, Rebbeca R. Chahine, Mathieu Bernard, Philippe Kowalczyk, Pierre Noe, and Olivier Thomas. New insights into thermomechanical behavior of GeTe thin films during crystallization. *Acta Materiala*, 191:60–69, 2020.

[49] RR Reeber and K Wang. Thermal expansion and lattice parameters of group IV semiconductors. *Materials Chemistry and Physics*, 46(2-3):259–264, 1996.

[50] H Watanabe, N Yamada, and M Okaji. Linear thermal expansion coefficient of silicon from 293 to 1000 K. *International Journal of Thermophysics*, 25(1):221–236, 2004.

[51] NA Pertsev and AG Zembilgotov. Domain populations in epitaxial ferroelectric thin films: Theoretical calculations and comparison with experiment. *Journal of Applied Physics*, 80(11):6401–6406, 1996.

[52] KS Lee and S Baik. Reciprocal space mapping of phase transformation in epitaxial PbTiO3 thin films using synchrotron x-ray diffraction. *Journal of Applied Physics*, 85(3):1995–1997, 1999.

[53] K Lee, KS Lee, and S Baik. Finite element analysis of domain structures in epitaxial PbTiO3 thin films. *Journal of Applied Physics*, 90(12):6327–6331, 2001.

[54] KS Lee, JH Choi, JY Lee, and S Baik. Domain formation in epitaxial Pb(Zr,Ti)O-3 thin films. *Journal of Applied Physics*, 90(8):4095–4102, 2001.